International Journal of Energy Production and Management
Vol. 10, No. 1, March, 2025, pp. 51-59
Journal homepage: http://iieta.org/journals/ijepm

Influence of Aluminium Anode Nanostructure on Ionic Conductivity and Battery Capacity

Firman Ridwan[1*], Dahyunir Dahlan[2], Dandi Agusta[1], Muhammad Akbar Husin[1]

[1] Department of Mechanical Engineering, Faculty of Engineering, Andalas University, Padang 25163, Indonesia
[2] Department of Physics, Faculty of Mathematics and Natural Sciences, Andalas University, Padang 25163, Indonesia

Corresponding Author Email: firmanridwan@eng.unand.ac.id

https://doi.org/10.18280/ijepm.100106

Received: 13 September 2024
Revised: 19 November 2024
Accepted: 14 February 2025
Available online: 31 March 2025

Keywords:
electron discharge rate, anode surface area, gel electrolyte, anodization, electrochemical performance

ABSTRACT

This research examines the influence of anode surface area on the efficacy of aluminium-air batteries. Three varieties of aluminium anodes were produced: non-mesh, one-step nanomesh, and two-step nanomesh. The nanomesh structures were fabricated via a multi-step anodization procedure employing phosphoric acid, leading to enhanced surface area and pore density. Scanning electron microscopy demonstrated that the 2-step nanomesh anode possessed the highest average pore diameter of 180 nm, resulting in a substantial enhancement of active surface area. Electrochemical characterization methods, such as galvanostatic discharge testing, electrochemical impedance spectroscopy, and cyclic voltammetry, were utilized to assess battery performance. The findings indicated that the 2-step nanomesh anode had superior electron discharge rate, ionic conductivity, and oxidation stability relative to the 1-step nanomesh and non-mesh anodes. The 2-step nanomesh anode attained a specific capacity of 1.92 mAh and a power output of 59.71 mW, exceeding the performance of alternative anode topologies. The improved battery performance is due to the enlarged active surface area of the anode, which promotes more efficient ion transport and electrochemical processes. The findings underscore the importance of anode surface modification in enhancing the performance of aluminium-air batteries and offer insights for the design of high-capacity, high-power energy storage systems for diverse applications.

1. INTRODUCTION

The continuous transition from a fossil fuel-dependent economy to cleaner energy alternatives is a critical component of contemporary society's endeavors to mitigate environmental contamination. Batteries are an option of alternative energy source that does not generate environmental contamination as a result of combustion. This transition has led to extensive exploration of renewable energy sources, including solar, wind, and hydropower. Moreover, in this evolving energy landscape, the development of safe, reliable, and efficient energy storage technologies is of paramount importance, especially for large-scale applications. Batteries, known for their relatively high energy density and electronic efficiency, are extensively used in portable electronic devices and electric vehicles (EVs) [1-4].

Within the realm of electrochemistry, the intricate interplay of ions in the electrolyte with the surfaces of the anode and cathode is profoundly influenced by several factors, including solution concentration, electrode surface area, current strength, stirring, and heating [5]. Notably, a larger active surface area holds a key role in enhancing reactivity, as it allows more surface atoms to interact with other substances [6]. To address this, the utilization of nanostructures, such as nanoporous materials, nanofibers, nanowhiskers, nano textures, nanomeshes, nanorods, nanosheets, nanoshells, and nanowires, has become a pivotal strategy in mitigating the challenges faced by all- solid-state batteries, particularly in improving the contact between electrodes and electrolytes [7-9]. This approach significantly amplifies the surface's active area, thereby promoting efficient electrochemical processes [10]. Furthermore, the concept of tortuosity has emerged as a crucial parameter in the study of porous media. Researchers have diligently strived to characterize the microstructure and ion transport properties of composite electrodes in batteries, as tortuosity provides insights into the intricacies of ion transport pathways within electrodes [11-14]. Higher tortuosity values indicate more complex transport routes for ions within electrodes, and this parameter is intricately linked to the high-rate charging and discharging characteristics of batteries. Past research endeavours have harnessed tortuosity as a predictive tool to gauge ion transport ease within electrodes and to understand how it influences battery output characteristics. For instance, Ebner et al. [15] harnessed the Bruggeman relationship to calculate the tortuosity of ion transport pathways within the electrode, taking into account the shape of the active material used in the battery.

Research into aluminium-air batteries has explored a wide spectrum of variables, encompassing aluminium anode concentrations, electrolyte membranes, and cathodes [16].

This research can be broadly categorized into two groups: those employing pure aluminium anodes and those utilizing alloy aluminium anodes.

In the pursuit of battery advancements, a notable study was conducted using high-purity 99.999% aluminium. Fan et al. [17] employed a 4 M NaOH electrolyte with air as the cathode. The results were promising, with a current density of 50 mA cm^2, a specific capacity of 2885 mAh/g, a voltage of 0.85 V, and an energy density of 2473 wH/kg. Additionally, Gelman et al. [18] explored the use of 99.997% aluminium with an air cathode, MnO_2/C, and EMIm (HF) 2.3F ionic liquid electrolyte, yielding a current density of 1.5 mA/cm^2, a specific capacity of 2100 mAh/g^1, a voltage of 1.1 V, and an energy density of 2300 wH/kg [19].

Recognizing the importance of aluminium alloy in mitigating corrosion, Levy et al. [20] employed a similar aluminium anode but with a TBAH2F3 ionic liquid/propylene carbonate electrolyte and air, along with MnO_2/C as the cathode. The results showed a current density of 0.5 mA cm^{-2}, a specific capacity of 1083 mAh/g, a voltage of 1.4 V, and an energy density of 1516 wH/kg.

Researchers discovered that the presence of aluminium impurities decreases the rate at which corrosion occurs by stimulating the surface of the anode. This finding has led researchers to explore the use of alloy anodes as a means to improve battery performance.

Indeed, research conducted by Ryu et al. [21] using aluminium alloy 6061 with an air/Ag_2MnO_4/C cathode and a 6 M KOH electrolyte achieved notable results, with a current density of 100 mA/cm^2, a specific capacity of 2834 mAh/g, a voltage of 0.9 V, and an energy density of 2552 wH/kg. Moreover, significant improvements in current density, voltage, and energy density were observed in the combination of an aluminium alloy anode (Mg–Sn-Ga-Si-Fe), O_2 cathode, MnO_2/C, and a 7 M KOH + 0.05 M Na_2SnO_3 electrolyte, as demonstrated by Wen et al. [22], yielding a current density of 140.9 mA/cm^2, a peak power density of 114.6 mW/cm^2, and an energy density of 4591 wH/kg.

In the end, the selection of aluminium alloy over pure aluminium is critical, as it has a direct impact on critical performance characteristics. While aluminium alloys exhibit greater current and energy density, unadulterated aluminium maintains the upper hand in terms of specific capacity and voltage. Nevertheless, the elevated corrosion rate of pure aluminium presents obstacles to its utilization as an anode with regards to electrochemical behavior and corrosion [23]. The results of this study underscore the significance of material choice in optimizing the performance of aluminium-air batteries.

From the previous research mentioned above, research on the influence of nanostructure on aluminium batteries, how the membrane fits the aluminium anode, capacity, and conductivity are questions that need to be solved. The objective of this study is to investigate the impact of anode surface area on the performance of porous anodes manufactured in three steps: non-nanomesh, 1-step nanomesh, and 2-step nanomesh. The study showed that the electron flow rate in the 2-step mesh was significantly higher compared to the 1-step mesh and non-mesh anodes. The 2-step Al-mesh anode showed excellent battery performance, achieving a capacity of 1.92 mAh and a power production capability of 59.71 mW. Aluminium alloy is utilized as the anode to prevent corrosion. The objective is to identify stable and efficient battery systems and to comprehend how relative differences in anode surface area affect ion transfer. The investigation encompassed a thorough electrochemical examination, which comprised cycle voltammetry, ionic conductivity, specific capacity, and the relationship between voltage and capacity, among other parameters.

Affordable aluminium batteries can be a potential alternative energy source for vehicles, including cars. This aluminium battery technology has the potential to support government policies in producing electric cars at more affordable prices. With lower production costs, electric vehicles can be accessed by more consumers, which in turn can accelerate the transition from fossil fuel vehicles. This will help reduce air pollution and greenhouse gas emissions caused by the combustion of fossil fuels, as well as contribute to global efforts to create a cleaner and more sustainable environment.

The structure of this paper is organized as follows: the Introduction provides the background, objectives, and significance of anode active surface area on the performance of aluminium-air batteries. The Experimental outlines the experimental approach and procedures used to examine the effects of anode surface area. The Results and Discussion section presents key findings and provides an in-depth analysis of these results. Finally, the Conclusion summarizes the main contributions of this study and its implications for advancing the design of more efficient aluminium-air batteries.

2. EXPERIMENT DESIGN

2.1 Materials

The investigation utilized PVA and TEOS acquired from Sigma-Aldrich, HCl and H_3PO_4 (85%) from Merck as the main constituents. The following chemicals were obtained from local suppliers: ethanol (96%), alcohol (96%), acetone (99%), NaOH (55%), and deionized water. Before utilization, every aluminium component underwent a degreasing process involving the application of NaOH, followed by submersion in acetone and ethanol for a duration of 15 minutes, and subsequently rinsed with distilled water.

2.2 Characterization measurement

The chemical composition and type of cement ash powder were evaluated using an XRF PANalytical Epsilon 3. The measurement of membrane impedance levels is conducted using Electrochemical Impedance Spectroscopy, specifically Electrochemical Impedance Spectroscopy (EIS), employs a Corrtest 100E Potentiostat that operates within a frequency range of 10 μHz to 1 MHz. The Potentiostat offers a high level of accuracy for both potential and current measurements, with an accuracy of 0.1% of the complete range. The minimum potential resolution is 10 mV, while the minimum current resolution is 100 fA. The Electrochemical Impedance Spectroscopy (EIS) was conducted under Potentiostatic conditions, with a frequency range of 10 mHz to 100 kHz. The applied voltage consisted of a direct current (DC) of 1 mV and an alternating current (AC) of 10 mVrms. The measurements were performed at room temperature, and a stabilization period of approximately 10 minutes was allowed. The electrolyte impedance (Z) was determined from the Nyquist plot, and this value was utilized to compute the ionic conductivity (σ) using the equation:

$$\sigma = \left(\frac{1}{\sqrt{Z_{re}^2+Z_{im}^2}}\right)1000 \quad (1)$$

Z_{re} represents the resistance of the membrane and Z_{im} represents the reactance of the membrane.

In order to evaluate the effectiveness of different gels as electrolytes in primary batteries, Al/air cells were tested under discharge conditions. The studies were conducted utilizing a Corrtest 100E Potentiostat, which consistently maintained a current density of 1, 2, 5, and 10 mA/cm² across a surface area of 4cm². After conducting the discharge test, the discharging time can be used to calculate the capacity (*C*) and capacity density (*CD*) of the battery using the equation:

$$Capacity = (I.t)A \quad (2)$$

$$CD = \frac{(I.t)A}{m} \quad (3)$$

I represent current, *t* is the discharging time, *A* is the anode surface area, and *m* is the anode mass

In addition, the materials were analyzed using Scanning Electron Microscopy (SEM) with a Hitachi S-3400N apparatus. This analysis aimed to provide information about the materials' microstructural and elemental properties.

2.3 Anode surface area simulation

The total surface area of the anode is calculated based on the following formula:

$$C_{Pore} = 2\pi rt \quad (4)$$

$$N_{pore} = \left(\frac{n}{1000000}\right)A \quad (5)$$

$$A_{total} = \left(C_{Pore}.N_{pore}\right) + A \quad (6)$$

C_{Pore} represents the circumference of the pore, N_{Pore} represents the total number of pores on the anode, *r* represents the radius of the pore, *t* represents the height of the pore, *n* represents the number of pores per 1 µm², and *A* represents the surface area of the anode without any pores. The surface area of the porous anode is determined by factors such as the size, depth, quantity, and spacing of its pores. The simulation assumes that the depth of the pore is twice the diameter of the pore. Typically, researchers restrict the anodizing operation to a maximum of 2 steps. Performing more than 2 steps of anodizing can harm the pore structure, hence hindering the attainment of larger pore diameters in the several stages. Indeed, it is important to enlarge the pore diameters by several stages in order to get the optimal surface area. Once the optimum point is reached, further increasing the pore diameter will result in a decrease in the electrode surface area. Hence, it is necessary to simulate the optimal surface area in order to calculate the electron transfer rate resulting from the anode's surface area.

2.4 Preparation of nanomesh

Low-purity 0.5 mm aluminium pieces were segmented into coupons measuring 30×20 mm². The aluminium pieces were first degreased using NaOH, followed by soaking in acetone and ethanol for 15 minutes, and finally cleaned with distilled water. The aluminium underwent anodization for a duration of 3 hours at a consistent temperature of 7°C, utilizing a solution containing 1 wt% of H_3PO_4. During the anodization process, there was a 19 mm gap between the anode and cathode. Following the 1-step anodization procedure, the aluminium surface was subsequently dried and cleansed with distilled water. Subsequently, a solution comprising 5 wt% H_3PO_4 was employed to corrode the aluminium surface for a duration of 60 minutes at ambient temperature. The anodization process was carried out in two stages, replicating the initial phase. An analysis was conducted on the shape and pore properties of the nano structures' membrane.

2.5 Preparation of gel electrolyte membrane

8 g of PVA was dissolved in 100 ml of distilled water at 80°C for 30 minutes while being agitated at 600 revolutions per minute to produce a solution. 36 g of HCl were added to the solution subsequent to the homogenization of the PVA. The mixture was stirred for an additional 30 minutes after TEOS was added, following 30 minutes of agitation to attain homogeneity. During the process of complete mixing, 1.6 g of cement particles are incorporated. The volume of the solution was brought to 75 ml during a 1-hour period of agitation while constant heat was applied. A battery case mold was utilized to construct an electrolyte membrane, which was achieved after 7 days of permitting the solution to rest at room temperature.

The aluminium battery production method comprises 3 types of aluminium anode (Al-non mesh, Al-1step nanomesh, and Al-2 step nanomesh), electrolyte, and carbon plate cathode. In order to assess the effectiveness of aluminium nanomesh anodes, Al-air batteries with a sandwich-like structure were produced. Figure 1 depicts the configuration of the assembled Al-air battery. The electrolyte membrane is situated between the Al-nanomesh and activated carbon. The overall flexibility of the battery is ensured by the flexibility of each individual component. Each of the three types of anodes were combined into 3 batteries and subjected to testing using a potentiostat.

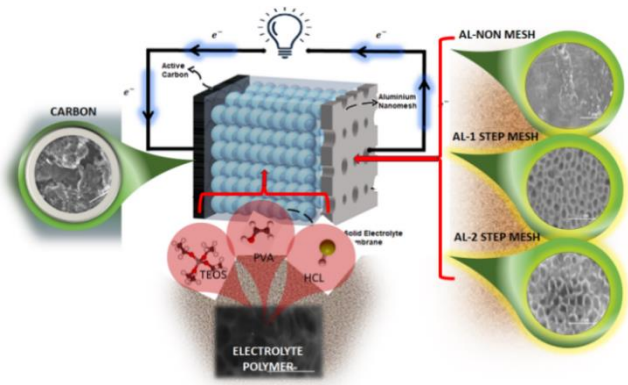

Figure 1. Step-by-step fabricating an aluminium air battery consists of a three-type aluminium anode and a gel electrolyte membrane

3. RESULT AND DISCUSSION

3.1 X-ray Fluorescence (XRF) test

X-ray Fluorescence (XRF) testing was used to assess the

chemical composition of aluminium alloys as shown in Figure 2. Figure 2 shows aluminium detected at approximately 1.5 keV, consistent with findings by Pinto et al. [24]. Table 1 presents the percentage composition of elements found in aluminium alloys. The major constituent of aluminium content is aluminium, along with important impurities including Copper (Cu), Iron (Fe), Silicon (Si), and other minor impurities. In addition, there are other minerals, such as manganese (Mn) and titanium (Ti).

Table 1. Chemical composition on aluminium alloy

Anode	Elements								
	Al (%)	Mn(%)	Si(%)	Ti(%)	V(%)	Cr(%)	Fe(%)	Ni(%)	Cu(%)
Aluminium Alloy	97.58	0.0051	0.63	0.047	0.024	0.007	0.726	0.017	0.224

3.2 Scanning electron microscope analysis

The process of anodizing aluminium using high concentrations of phosphoric acid is a widely employed method for creating nanomesh membrane [25]. Nevertheless, the investigation involved anodizing aluminium samples in a 1 wt% H_3PO_4 solution. The anodization process was carried out at a voltage of 100 V and a temperature of 10°C, using an ice bath for temperature control. Figure 3 displays scanning electron microscope (SEM) images of nonmesh and nanomesh membranes following both 1-step and 2-step anodization processes. The nanomesh is observed from a top-down perspective. The electric field is augmented by a voltage of 100 V in 1-step anodization, which in turn accelerates the corrosion process on aluminium. Consequently, the partition barriers between the pores become thinner. Etching is a controlled corrosion process using H_3PO_4. The chemical etching procedure is conducted for one hour to smooth the surface of the pores. By increasing the surface area of the pores, etching can more clearly display the geometry of the nanomesh and the number of pores. The pores become larger as the etching time increases [26, 27]. Nevertheless, the corrosion rate is increased in the nanomesh produced through the 2-step anodization process, resulting in larger apertures than those of the 1-step process.

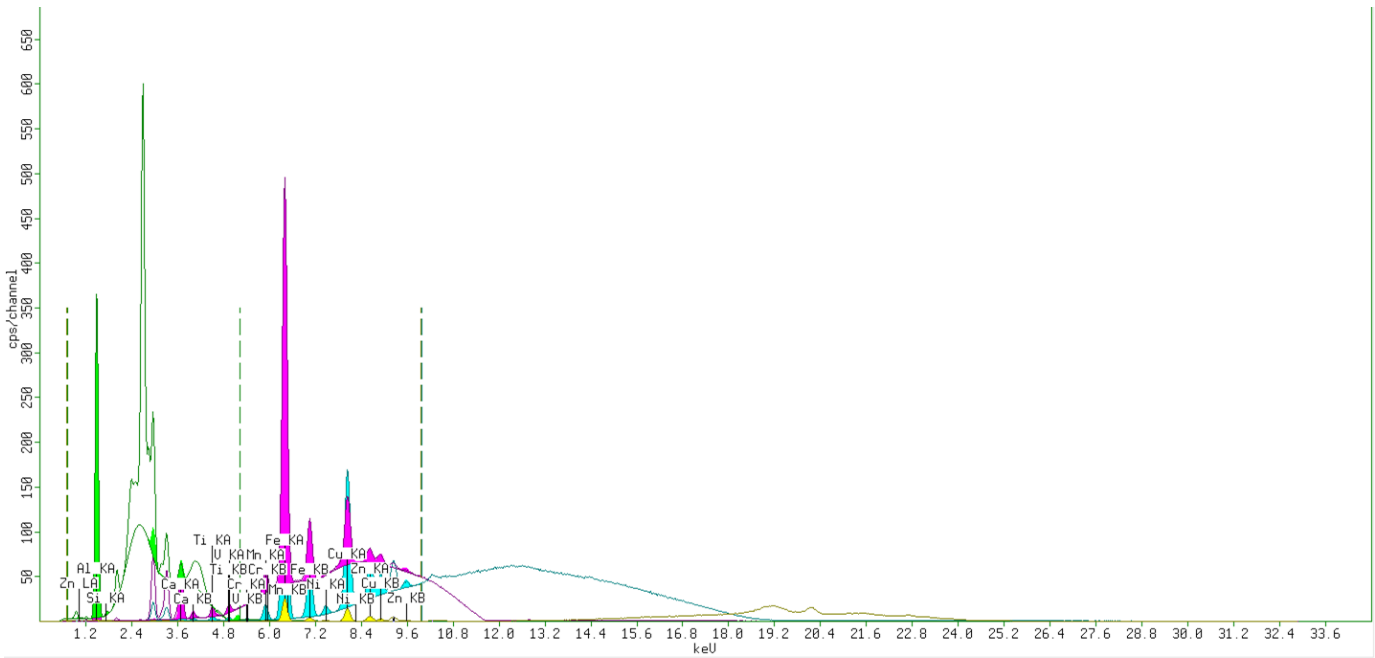

Figure 2. Aluminium test results with XRF

These results indicate that the surface area of the 2-step nanomesh is more extensive than the 1-step nanomesh and the non-mesh. As previously mentioned, surface area significantly influences electron transfer [28]. Furthermore, the aluminium anode is referred to as the non-mesh, 1-step-mesh, and 2-step-mesh for the non-mesh, 1-step anodizing and 2-steps anodizing aluminium anode, respectively.

Figure 3 (a) shows an aluminium anode before undergoing anodization treatment. Figure 3 (c) and (d) depict aluminium anodes that have undergone 1 and 2-step-mesh procedures, resulting in varying pore sizes. The subsequent anodization process leads to an increase in the diameter of the pores. The electron transport is strongly affected by the pore size of the aluminium anode. Increased pore size enhances electron mobility, as demonstrated by a decrease in resistivity [29]. Figure 3 (e) and (f) show the average pore diameter distribution for 1 and 2 step-mesh respectively.

Figure 3 (b) shows the SEM image of the gel electrolyte membrane sample formed by stirring-heating and evaporation process. It can be seen that membrane has some spots that made on it. It was a charred solution that mixed in the solution. Charring occurs because the heating process to remove the moisture content is done long enough and the bottom part runs out of water. Although the water has thinned, the solution can still be agitated. The solution that has been charred and hardened is also agitated and becomes an impurity.

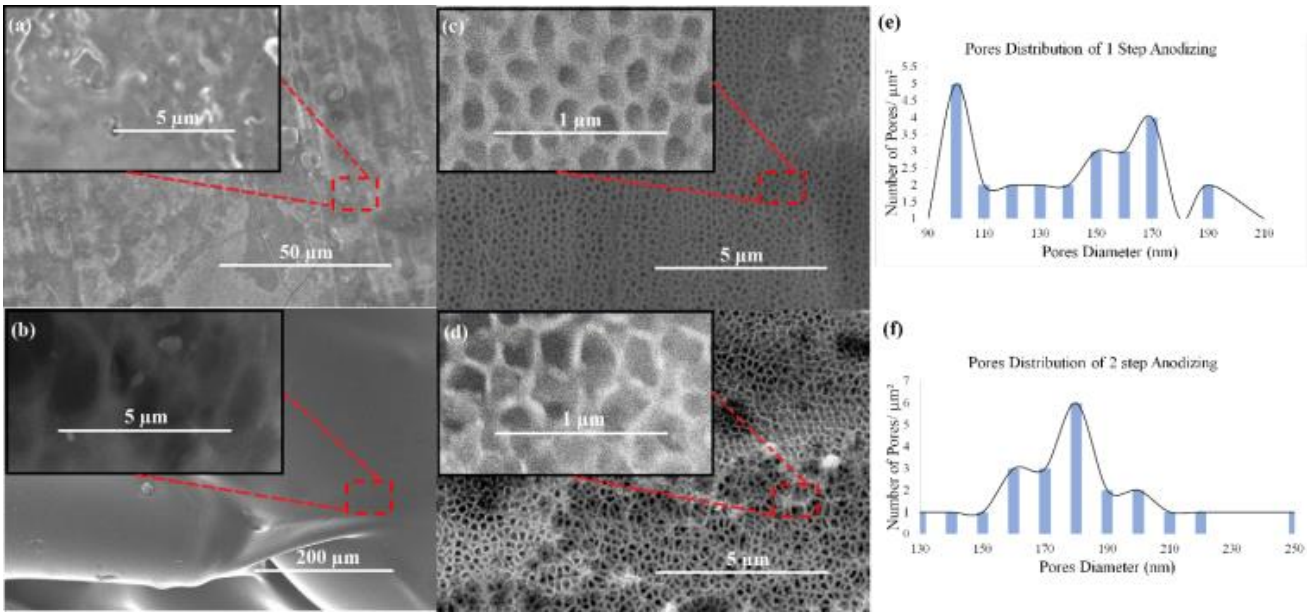

Figure 3. SEM images of (a) non-mesh, (b) membrane electrolyte, (c) 1-step-mesh, (d) 2-step-mesh, (e) pore distribution of 1-step-mesh, and (f) pore distribution of 2-step-mesh

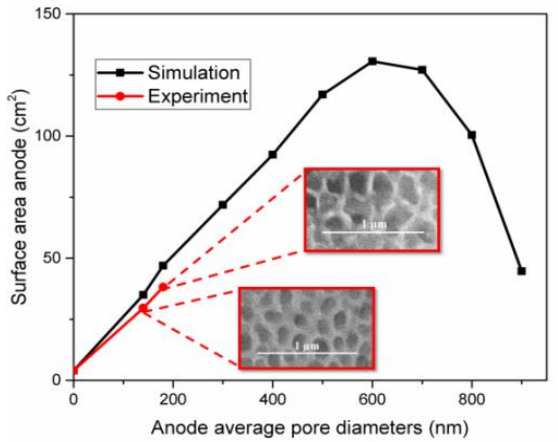

Figure 4. Surface area anode

Researchers in the subject of anodizing commonly employ either a 1-step or 2-step technique, with no cases of anodizing beyond two steps. It is not feasible to ascertain the optimal surface area of the anode by more than two steps of anodizing. Hence, the calculation of the optimal surface area simulation is derived from the Eqs. (4)-(6). Figure 4 illustrates the optimal surface area as a function of the increase in diameter, depth, and number of pores for both 1 and 2 step mesh processes.

3.3 Discharging

The impact of aluminium surface area on the discharge performance of a battery consisting of a carbon plate as the cathode and aluminium as the anode is illustrated in Figure 5. The discharge performance of a battery equipped with a non-mesh aluminium anode is shown in Figure 5(a). The galvanostatic test graph shows that discharge at 1 mA begins at 1.33 V and continues for 274.13 seconds. Charging at 2 mA starts at 1.32 V and lasts 173.5 seconds. The voltage and duration of battery operation decreases as the discharge amperes increase. The discharge performance of a battery equipped with an aluminium anode subjected to a 1-step mesh is illustrated in Figure 5(b). The galvanostatic test graph shows that a battery with an initial voltage of 1.37 V lasts for 422.46 seconds when discharged by 1 mA. In contrast to non-porous anodes, 1-step-mesh aluminium exhibits increased operating time and battery voltage. One of the anodization phases forms pores on the surface of the aluminium plate, thereby increasing the surface area of the plate. This phenomenon indicates that the electron flow rate depends on the surface area of the electrode, as evidenced by the increase in conductivity and battery capacity [30]. The performance of a battery equipped with a 2-step-mesh anode is depicted in Figure 5 (c). These findings demonstrate substantial improvements in battery operational capabilities. In a 1 mA galvanostatic discharge test, the battery shows a discharge time of 1735.16 seconds from an initial voltage of 1.31 V. At 2 mA, the battery shows a discharge time of 907.16 seconds from a voltage of 1.34 V. At 5 mA, the battery shows a discharge time 907.16 seconds from an initial voltage of 1.34 V. The discharge time is reduced to 387.13 seconds from a voltage of 1.37 V. Finally, at 10 mA, the discharge time is 157.06 seconds from a voltage of 1.34 V. Using Eq. (2) and Eq. (3), the battery's electrical capacity was calculated, with the highest capacity of 1.92 mAh achieved by the battery with a 2-step mesh anode. During the discharge test with a 2-step-mesh anode, there is a significant increase in power supply. Nevertheless, this research shows that increasing the surface area of the anode (especially aluminium) can result in more efficient ion transfer, as evidenced by an increase in the electrical capacity of the battery [31].

3.4 Electrochemical impedance spectroscopy

Figure 6 (a) illustrates that the impedance graph appears as a linear line at low frequencies and as a semicircle at high frequencies. The Nyquist plot depicts the impedance of the battery with an aluminium non-mesh, as well as aluminium 1 and 2-step-mesh. The plot covers a frequency range from 10 mHz to 10 kHz. At lower frequencies, the rate of ion transfer from the battery reduces, resulting in an increase in the Nyquist curve. Enhancing the surface area of the aluminium (anode) will enhance the curve, particularly at lower frequencies. The resistance fluctuation curves, both real and imaginary, exhibit a reduction with an increase in the surface

area of the anode. The outcome is that the semicircular curve enhances. The rationale for this is that a larger surface area of the anode in contact with the gel electrolyte facilitates more frequent and efficient collisions, thereby enhancing the reaction rate [32]. If the reaction rate increases, a greater quantity of ions will be generated from the battery. The ionic conductivity of each membrane can be calculated by utilising the impedance value and cross-sectional area of the electrode.

The battery with the largest-pore anode has the lowest impedance at 171.65 Ω, as shown in Figure 6(a). Based on Nyquist data, the ionic conductivity is calculated using Eq. (1), resulting in a value of 0.00147 S/cm for the anode with the largest pores, as shown in Figure 6(b). In contrast, the non-porous anode shows a significant decrease in conductivity around 0.00058 S/cm. Since the number of pores is proportional to the anode's surface area, it can be concluded that increasing the anode's surface area enhances its ionic conductivity.

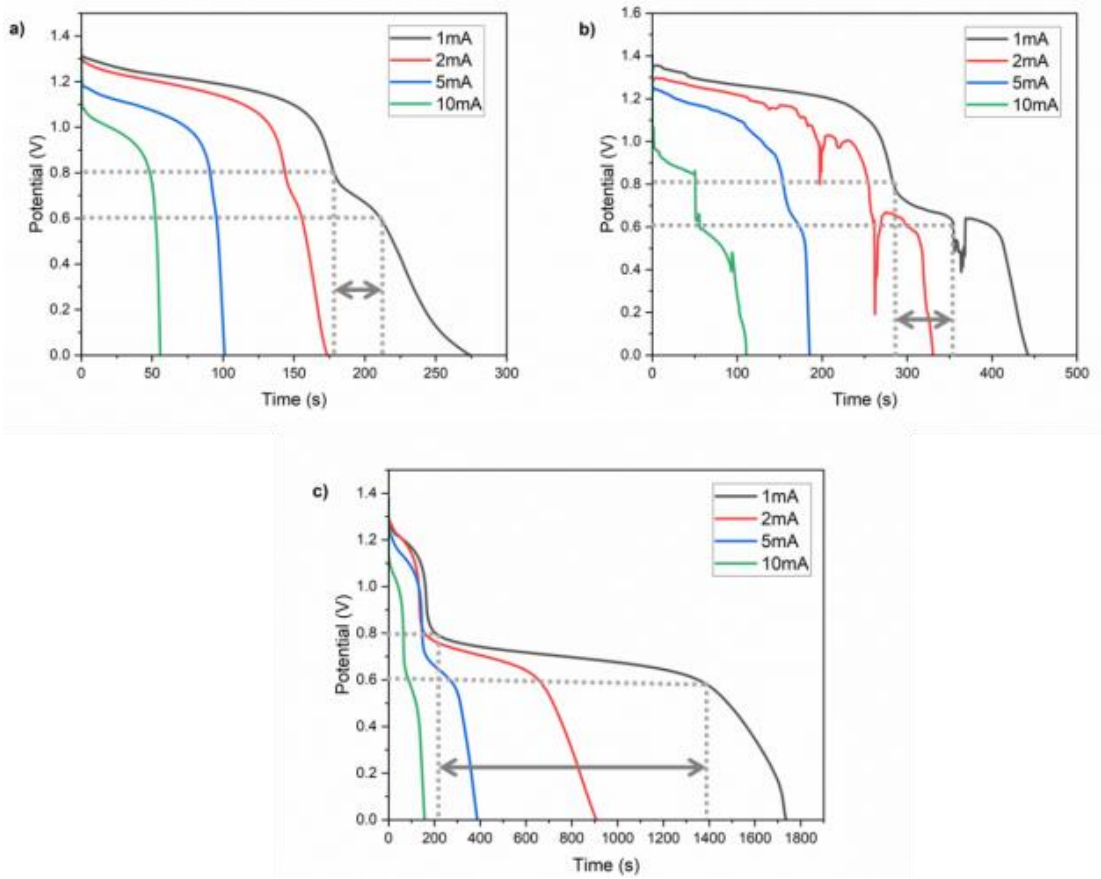

Figure 5. Effect of anode (a) non-mesh (b) 1-step-mesh, (c) 2-step-mesh on battery performance during galvanostatic discharge testing with constant amperes varying 1 mA, 2 mA, 5 mA and 10 mA.

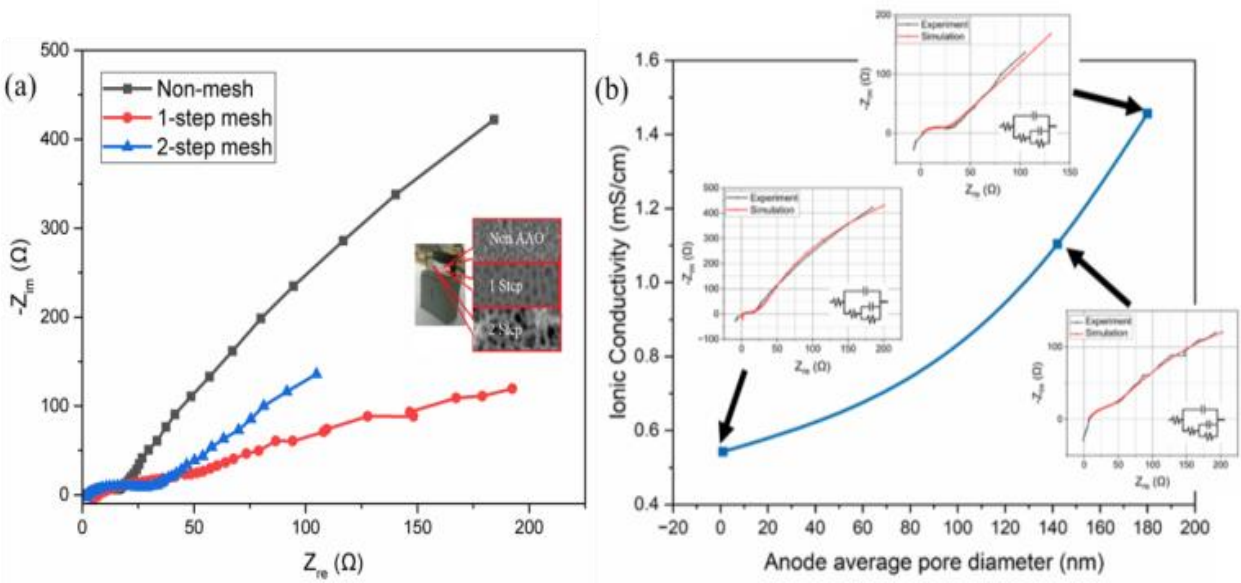

Figure 6. Three types aluminium anode (a) Nyquist plot of a battery with non-mesh anode, 1-step-mesh anode and 2-step-mesh (b) Ionic conductivity

3.5 Cyclic voltammetry

By performing cyclic voltammetry studies, the chemical and electrochemical stability of polymer electrolyte membranes can be determined through the measurement of ionic conductivity. The voltammetry cycle of an aluminium air battery is illustrated in Figure 7. 2-step-mesh aluminium anode batteries exhibit the most significant peak oxidation current and voltage, at 10.077 mA and 1.5 V, respectively. Peak oxidation voltage decreases proportionally to the surface area of the anode. An instance of the 1-step-mesh aluminium anode yields a maximum oxidation current of 9.75 mA and a voltage of 1.02 V. A non-mesh aluminium anode with 0.88 V and 8.5 mA of oxidation current and voltage, respectively. This property indicates that by augmenting the anode's surface area, the oxidation process can be prolonged. The discharging and cyclic voltammetry tests yielded various battery parameters which demonstrates a 2-step-mesh anode that has the highest possible electrical capacity and specific capacity, which are 1.92 mAh and 2.71 mAh/g, respectively. This is succeeded by the battery with the 1-step nanomesh anode and the non-mesh anode, which have values of 0.49 mAh, 0.69 mAh/g and 0.3 mAh, 0.42 mAh/g, respectively as concluded in Table 2.

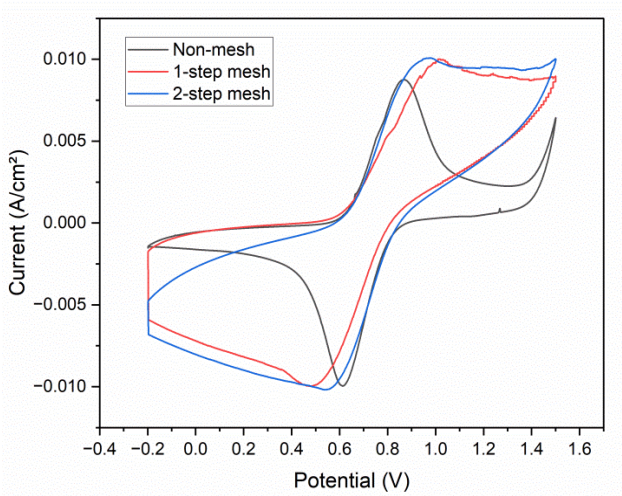

Figure 7. Cyclic voltammetry of an aluminium air battery

Table 2. Battery performance

Anode	Power (mW)	Power Density (mW/cm²)	Capacity (mAh)	Specific Capacity (mAh/g)
Non-mesh	36.81	9.20	0.3	0.42
1-step-mesh	53.28	13.32	0.49	0.69
2-step-mesh	59.71	14.92	1.92	2.71

Table 2 illustrates the relationship between anode surface area and variations in pore distribution and pore diameter. Larger pores contribute to higher capacity and power, while aluminium anodes without mesh have a smaller surface area, resulting in the lowest battery capacity and power. A larger surface area of the anode will result in the release and transport of a greater number of ions [33, 34].

4. CONCLUSIONS

The research discussed in the entry focuses on the impact of anode surface area on the electron discharge rate in a battery. This research compares the performance of 3 types of anodes: non-mesh anodes and 2 types of aluminium nanomesh anodes. The nanomesh structure increases the active surface area of the anode, causing a more dispersed distribution of electron discharge. The anode is subjected to 1-step and 2-step anodizing operations to differentiate the active surface area. The study found that the 2-step anodization process generates a more intricate nanomesh structure, characterized by an average pore diameter of 180 nm, which leads to a significant augmentation in the active surface area of the anode. The research findings show that the 2-step-mesh anode has a much higher electron discharge rate compared to the 1-step-mesh and non-mesh anodes. The research results show that increasing the anode surface area will prolong the oxidation process. The 2-step-mesh anode shows relatively better battery performance, with a specific capacity of 1.92 mAh and the ability to provide 59.71 mW of power. Overall, the research shows that increasing the active surface area of the anode through the use of nanomesh structures can significantly increase the electron discharge rate and battery performance. This has implications for the development of more efficient and reliable energy storage technologies, especially in the context of renewable energy sources and electric vehicles. This study explains how the anode active surface area enhances the electron release efficiency of aluminium-air batteries. This study concentrates on the size of the anode surface, in contrast to previous research that examined electrolyte materials or the composition of electrode materials. These results corroborate previous research and the exploration of optimal electrode design, indicating a path toward more efficient and durable aluminium-air batteries for various applications.

FUNDING

This research is financed by: Directorate General of Higher Education, Research, and Technology Ministry of Education, Culture, Research, and Technology, Indonesia in accordance with the research contract No.: 190/E5/PG.02.00.PT/2022 Fiscal year 2022.

AUTHOR CONTRIBUTIONS

Firman Ridwan: Conceptualization, Methodology, Validation, and Supervision, Dandi Agusta: Data Curation, Investigation, and Writing original draft. Muhammad Akbar Husin: Visualization and Software. Dahyunir Dahlan: Formal Analysis, Supervision.

COMPETING INTERESTS

The authors declare that they have no known competing financial interests or personal relationships that could have appeared to influence the work reported in this paper.

REFERENCES

[1] Dunn, B., Kamath, H., Tarascon, J.M. (2011). Electrical energy storage for the grid: A battery of choices. Science, 334(6058): 928-935. https://doi.org/10.1126/science.1212741

[2] Tie, S.F., Tan, C.W. (2013). A review of energy sources and energy management system in electric vehicles. Renewable and Sustainable Energy Reviews, 20: 82-102. https://doi.org/10.1016/j.rser.2012.11.07

[3] Pollet, B.G., Staffell, I., Shang, J.L. (2012). Current status of hybrid, battery and fuel cell electric vehicles: From electrochemistry to market prospects. Electrochimica Acta, 84: 235-249. https://doi.org/10.1016/j.electacta.2012.03.172

[4] Mandrile, F., Martino, M., Musumeci, S., Pastorelli, M. (2023). Hybrid battery systems: An investigation for maritime transport. International Journal of Energy Production and Management, 8(3): 141-147. https://doi.org/10.18280/ijepm.080302

[5] Shi, J., Jiang, B., Liu, Z., Li, C., Yan, F., Liu, X., Li, H., Yang, C., Dong, D. (2021). Effects of specific surface area of electrode and different electrolyte on capacitance properties in nano porous-structure CrN thin film electrode for supercapacitor. Ceramics International, 47(13): 18540-18549. https://doi.org/10.1016/j.ceramint.2021.03.177

[6] Connor, P., Schuch, J., Kaiser, B., Jaegermann, W. (2020). The determination of electrochemical active surface area and specific capacity revisited for the system MnOx as an oxygen evolution catalyst. Zeitschrift für Physikalische Chemie, 234(5): 979-994. https://doi.org/10.1515/zpch-2019-151

[7] Park, S.Y., Jeong, J., Shin, H.C. (2022). Geometrical effect of active material on electrode tortuosity in all-solid-state lithium battery. Applied Sciences, 12(24): 12692. https://doi.org/10.3390/app122412692

[8] Chen, R.J., Zhang, Y.B., Liu, T., Xu, B.Q., Lin, Y.H., Nan, C.W., Shen, Y. (2017). Addressing the interface issues in all-solid-state bulk-type lithium ion battery via an all-composite approach. ACS Applied Materials & Interfaces, 9(11): 9654-9661. https://doi.org/10.1021/acsami.6b16304

[9] Ding, Z., Li, J., Li, J., An, C. (2020). Interfaces: Key issue to be solved for all solid-state lithium battery technologies. Journal of The Electrochemical Society, 167(7): 070541. https://doi.org/10.1149/1945-7111/ab7f84

[10] Kim, H., Kim, M.C., Kim, S.B., Kim, Y.S., Choi, J.H., Park, K.W. (2020). Porous SnO_2 nanostructure with a high specific surface area for improved electrochemical performance. RSC Advances, 10(18): 10519-10525. https://doi.org/10.1039/d0ra00531b

[11] Bae, C.J., Erdonmez, C.K., Halloran, J.W., Chiang, Y.M. (2013). Design of battery electrodes with dual-scale porosity to minimize tortuosity and maximize performance. Advanved Materials, 25(9): 1254-1258. https://doi.org/10.1002/adma.201204055

[12] Bielefeld, A., Weber, D.A., Janek, J. (2020). Modeling effective ionic conductivity and binder influence in composite cathodes for all-solid-state batteries. ACS Applied Materials & Interfaces, 12(11): 12821-12833. https://doi.org/10.1021/acsami.9b22788

[13] Patel, K.K., Paulsen, J.M., Desilvestro, J. (2003). Numerical simulation of porous networks in relation to battery electrodes and separators. Journal of power Sources, 122(2): 144-152. https://doi.org/10.1016/S0378-7753(03)00399-9

[14] Wu, J., Ju, Z., Zhang, X., Takeuchi, K.J., Marschilok, A.C., Takeuchi, E.S., Yu, G. (2021). Building efficient ion pathway in highly densified thick electrodes with high gravimetric and volumetric energy densities. Nano Letters, 21(21): 9339-9346. https://doi.org/10.1021/acs.nanolett.1c03724

[15] Ebner, M., Chung, D.W., García, R.E., Wood, V. (2014). Tortuosity anisotropy in lithium-ion battery electrodes. Advanced Energy Materials, 4(5): 1-6. https://doi.org/10.1002/aenm.201301278

[16] Ma, D., Li, J., Li, H., Yuan, D., Ji, Z., Manawan, M., de León Albarran, C.P., Wu, C., Pan, J.H. (2024). Progress of advanced cathode materials of rechargeable aluminum-ion batteries. Energy Material Advances, 5: 0088. https://doi.org/10.34133/energymatadv.0088

[17] Fan, L., Lu, H. (2015). The effect of grain size on aluminum anodes for Al–air batteries in alkaline electrolytes. Journal of Power Sources, 284: 409-415. https://doi.org/10.1016/j.jpowsour.2015.03.063

[18] Gelman, D., Shvartsev, B., Ein-Eli, Y. (2014). Aluminum–air battery based on an ionic liquid electrolyte. Journal of Materials Chemistry A, 2(47): 20237-20242. https://doi.org/10.1039/C4TA04721D

[19] Zhu, N., Zhang, K., Wu, F., Bai, Y., Wu, C. (2021). Ionic liquid-based electrolytes for aluminum/magnesium/sodium-ion batteries. Energy Material Advances, 2021: 9204217. https://doi.org/10.34133/2021/9204217

[20] Levy, N.R., Lifshits, S., Yohanan, E., Ein-Eli, Y. (2020). Hybrid ionic liquid propylene carbonate-based electrolytes for aluminum–air batteries. ACS Applied Energy Materials, 3(3): 2585-2592. https://doi.org/10.1021/acsaem.9b02288

[21] Ryu, J., Jang, H., Park, J., Yoo, Y., Park, M., Cho, J. (2018). Seed-mediated atomic-scale reconstruction of silver manganate nanoplates for oxygen reduction towards high-energy aluminum-air flow batteries. Nature Communications, 9(1): 3715. https://doi.org/10.1038/s41467-018-06211-3

[22] Wen, H., Liu, Z., Qiao, J., Chen, R., Qiao, G., Yang, J. (2020). Ultrahigh voltage and energy density aluminum-air battery based on aqueous alkaline-acid hybrid electrolyte. International Journal of Energy Research, 44(13): 10652-10661. https://doi.org/10.1002/er.5707

[23] Wang, J.M., Wang, J.B., Shao, H.B., Zeng, X.X., Zhang, J.Q., Cao, C.N. (2009). Corrosion and electrochemical behaviors of pure aluminum in novel KOH-ionic liquid-water solutions. Materials and Corrosion, 60(12): 977-981. https://doi.org/10.1002/maco.200905238

[24] Pinto, A.H. (2018). Portable X-ray fluorescence spectrometry: Principles and applications for analysis of mineralogical and environmental materials. Aspects in Mining & Mineral Science, 1(2): 1-6. https://doi.org/10.31031/amms.2018.01.000506

[25] Lin, B., Chen, J., Kannan, P., Zeng, Y., Qiu, B., Guo, L., Lin, Z. (2019). Rapid synthesis of a highly active and uniform 3-dimensional SERS substrate for on-spot sensing of dopamine. Microchimica Acta, 186: 1-9. https://doi.org/10.1007/s00604-019-3357-1

[26] Le Coz, F., Arurault, L., Fontorbes, S., Vilar, V., Datas,

L., Winterton, P. (2010). Chemical composition and structural changes of porous templates obtained by anodising aluminum in phosphoric acid electrolyte. Surface and Interface Analysis, 42(4): 227-233. https://doi.org/10.1002/sia.3199

[27] Masuda, H., Yada, K., Osaka, A. (1998). Self-ordering of cell configuration of anodic porous alumina with large-size pores in phosphoric acid solution. Japanese Journal of Applied Physics, 37(11A): L1340. https://doi.org/10.1143/JJAP.37.L1340

[28] Zhang, C., Yi, P., Peng, L., Lai, X., Chen, J., Huang, M., Ni, J. (2017). Continuous fabrication of nanostructure arrays for flexible surface enhanced Raman scattering substrate. Scientific Reports, 7(1): 39814. https://doi.org/10.1038/srep39814

[29] Rizkia, V., Soedarsono, J.W., Munir, B., Suharno, B. (2017). An analysis of the electrolyte resistivity effect on the pore diameter and pore density of Anodic Aluminum Oxide (AAO) films produced by single-step anodization. International Journal of Technology, 8(8): 1479-1488. https://doi.org/10.14716/ijtech.v8i8.742

[30] Raeisi-Kheirabadi, N., Nezamzadeh-Ejhieh, A., Aghaei, H. (2022). Cyclic and linear sweep voltammetric studies of a modified carbon paste electrode with nickel oxide nanoparticles toward tamoxifen: Effects of surface modification on electrode response kinetics. ACS Omega, 7(35): 31413-31423. https://doi.org/10.1021/acsomecccga.2c03441

[31] Harrington, T.D., Babauta, J.T., Davenport, E.K., Renslow, R.S., Beyenal, H. (2015). Excess surface area in bioelectrochemical systems causes ion transport limitations. Biotechnology and Bioengineering, 112(5): 858-866. https://doi.org/10.1002/bit.25500

[32] Grewal, M.S., Kisu, K., Orimo, S.I., Yabu, H. (2022). Increasing the ionic conductivity and lithium-ion transport of photo-cross-linked polymer with hexagonal arranged porous film hybrids. Iscience, 25(9): 104910. https://doi.org/10.1016/j.isci.2022.104910

[33] Karamzadeh, M., Kadivarian, H., Kadivarian, M., Kazemi, A. (2020). Modeling the influence of substrate concentration, anode electrode surface area and external resistance in a start-up on the performance of microbial fuel cell. Bioresource Technology Reports, 12: 100559. https://doi.org/10.1016/j.biteb.2020.100559

[34] Wang, H., Yu, W., Mao, N., Shi, J., Liu, W. (2016). Effect of surface modification on high-surface-area carbon nanosheets anode in sodium ion battery. Microporous and Mesoporous Materials, 227: 1-8. https://doi.org/10.1016/j.micromeso.2016.02.003